Morphometric signature of sediment particles reveals the source and emplacement mechanisms of submarine landslides

S.K.M. Li[1], L. Zuo[2], V. Nardelli[3], T.M. Alves[4], S.D.N. Lourenço[1#]

[1] Department of Civil Engineering, The University of Hong Kong
[2] Department of Civil Engineering, School of Human Settlements and Civil Engineering, Xi'an Jiaotong University, Xi'an, China (formerly The University of Hong Kong)
[3] ONLYgeotechnics, Hong Kong (formerly The University of Hong Kong)
[4] School of Earth and Ocean Sciences, Cardiff University
[#] Corresponding author

Abstract

The long travel distances recorded by most submarine landslides indicate that changes in particle attributes (shape and size) may occur during their movement. Yet, little is known about the magnitude of such changes, and their underlying physical drivers. In order to understand the failure characteristics of submarine landslides, a dynamic image analyzer was used to characterize the particle size(s), aspect ratio, sphericity and convexity of 200 samples recovered from two IODP sites (C0018 and C0021) offshore Nankai (SE Japan). The two IODP sites drilled a series of submarine landslides, and undisturbed slope sediment, previously characterized in detail on 3D seismic data. The results of this work reveal no perceptive differences for particle size and shape between landslide and undisturbed slope strata, suggesting that remobilized sediment, sourced from marine deposits accumulated on the upper slope of Nankai do not change through slope instability. This lack of particle attribute differences between remobilized (landslide) and undisturbed sediment, and between the two IODP Sites, suggests limited interaction between particles during their movement. A fluidization mechanism is therefore proposed whereby the soft and saturated state of deep-sea sediment leads to the development of excess pore water pressure. This mechanism maintains movement and inhibits particle-to-particle contact, limiting subsequent particle shape and size variations in the failed sediment.

Keywords

SE Japan; submarine landslides; particle shape; particle size; emplacement; triggering

1. Introduction

Both terrestrial and submarine landslides are transported downslope as a mainly solid mass or as a flow and may impact the particle size and shape of the mobilized mass (Cruden and Varnes, 1974; Masson, 2016). During their movement, particles may collide, roll or slide past each other. Particle breakage has been identified within the shear surfaces of some terrestrial landslides, a phenomenon producing low-permeability layers that generate excess pore water pressure and enhance mobility (Wafid et al., 2004). In submarine landslides, little is known about particle attributes and landslide dynamics. Using drained and undrained ring shear tests, Wiemer and Kopf (2017) demonstrated that particle shape (rounded vs angular) and the surface texture (smooth vs rough) has a limited influence on the behavior of marine sediment under shear. The mineralogy, i.e. the presence volcanic ash vs pumice sands, was seen to dominate the response of marine sediment at high strains, with pumice sands exhibiting a higher potential for breakage and excess pore water pressure generation. Similar conclusions were also achieved in Wiemer et al. (2015), who found that basal slip surface were more likely to be located in relatively brittle diatomaceous sediments, rather than in volcanic ash.

The long travel distance of submarine landslides suggests that particle attributes (shape and size) alterations could occur but this has not been confirmed yet. At high strains, particle breakage is possible for coarser materials but depends on the vertical stress (overburden), pore water pressure (hydrostatic or in excess of the hydrostatic) and mineralogy. For clays, platelets are known to realign parallel to the shear surface after large shear displacements (Skempton, 1985). In fact, the generation of fines in the natural environment has been mostly explored in the literature referring to wind and river dynamics. For wind erosion, the generation of fines results from spalling, chipping and breakage of particles, in a process that includes the removal of grain coatings (Bullard et al., 2004). Kuenen (1960) found positive relationships between rates of aeolian abrasion and increasing particle size, angularity and surface roughness.

This work uses data taken from a dynamic image analyzer to elucidate the dynamics of submarine landslides. It concludes on particle attributes alterations, particle size, aspect ratio, sphericity and convexity by testing 200 samples taken from the International Ocean Discovery Program (IODP) boreholes C0018A (site C0018, borehole A) and C0021B (site C0021, borehole B) offshore Nankai Trough, SE Japan (Figs. 1a and 1b). The samples intercept a known sequence of submarine landslides or Mass Transport Deposits (MTDs A and B) and confining (undeformed) slope strata (Figs. 2a and 2b). The focus will be on MTD B in this work, and slope sediments confining it. As landslide deposits are important markers of tectonic movements (Alves et al., 2014), at the same time constituting important geohazards on continental margins, it is crucial to understand the emplacement mechanisms of such strata, and the internal character of landslide deposits after they are accumulated in mid and lower slope regions. A key driver for this work was the need to present a benchmark methodology to characterize submarine landslides, not only offshore Japan but also on other continental margins.

2. Site location

a) Sampling locations

Sediment samples were collected from two IODP boreholes: borehole C0021B (site C0021,Expedition 338 Scientific Party, 2013) located on the upper slope of Nankai, and borehole C0018A (site C0018,Expedition 333 Scientific Party, 2011) located on the mid slope of the same region (Fig. 1). A total of 101 samples (each around 5 grams) were

collected from each borehole, ranging from -90 m to -190 m below the sea floor. In addition, the mineralogy of two sediment samples from IODP Site C0021 was determined through X-ray diffraction analyses.

b) Internal character of MTD B based on seismic data

The Nankai accretionary complex results from the subduction of the Philippine Sea plate beneath the Eurasian plate along the Nankai Trough. The area comprises a submarine channel system and a mass-transport deposit B (MTD B, Expedition 333 Scientists, 2011) generated in a broad zone of deformation within the thrust zone. Sites C0021 and C0018, where the MTD B is located, comprise of silty mud and silty turbidites with several ash layers (Kimura et al., 2011). MTD B covers more than 20 km^2 and has a maximum thickness of ~182 m (Strasser et al., 2011).

The modern tectonic and depositional settings of the upper slope of Nankai were initiated at ~ 2.2 Ma in a frontal wedge-toe position (Strasser et al., 2009). Splay fault movement was initiated at ~ 1.95 Ma in the lower part of the accretionary wedge. Slip on a Megasplay Fault has occurred since ~ 1.55 Ma (Strasser et al., 2009), but displacement ceased at ~ 1.24 Ma towards its eastern part, suggesting a relatively short period of high activity between ~ 1.55 and 1.24 Ma in most of Nankai. Complementing these results, Gulick et al. (2010) recognized a major phase of landward tilting in the Kumano Basin, a basin located landward of the study area, and inferred activity of the Megasplay Fault between 1.3 and 1.0 Ma. MTD B was interpreted as a single event that transported the slide mass relatively rapidly as opposed to a relatively slow-moving cohesive landslide (Moore and Sawyer, 2016).

c) Mineralogy

The sediments sampled from IODP Sites C0018 and C0021 were previously classified as clayey silts, with a number of samples described as silty clays (Moore and Sawyer, 2014). The sediment fractions determined by the latter authors were sand (2.3%), silt (54.1%) and clay (43.6%). Minerals identified include quartz (58%), feldspar (albite, 18%), mica (muscovite, 18%) and smaller amounts of calcite, clinochlore and tremolite. These values are average percentages for both the samples. As it can be observed, quartz and feldspar are the prevalent fractions in the samples, a character typical of silty sediments as previously reported by Blaker et al. (2016) for the Halden silt, in the Halden Research Site, with the material originated from marine deposition. Other marine sediments from Asia are characterized by a clayey nature, and they contain high amounts of either kaolinite (Singapore clay; Bo et al., 2015) or smectite (Bangkok clay; Ohtsubo et al., 2000).

3. Methods

a) Particle attribute descriptors

A dynamic image analyzer (QICPIC™, Sympatec GmbH, Clausthal-Zellerfeld, Germany) was used to characterize particle attributes. The device comprises a gravity dispenser and a feeding device that controls the number of particles in contact with the laser beam, per unit time. A series of frames is then captured by a camera from which particle size and shape aremeasured. The feed and frame rate were adjusted to 30% and 50 Hz respectively.

The aspect ratio as defined by the dynamic shape analyzer QICPIC™ is the ratio of minimum to maximum Feret diameters, varying between 0 and 1. The Feret diameter is the length between two parallel lines tangential to a particle's silhouette (Fig. 3a). In parallel, the

value of sphericity is the ratio of perimeters for a given area and is equivalent to the 'degree of circularity' defined by Wadell (1933), in which P_{eqpc} is the perimeter of the equivalent circle and P_{real} is the actual perimeter. It can be deduced that the more the particle's 2D outline deviates from a circle, the larger P_{real} is. Thus, values of sphericity approaching 1.0 correspond to a shape close to a sphere (Fig. 3b). Convexity is the ratio between the projected area of a particle and the area of a convex shape. It is equal to the area A / area (A+B). The maximum value of convexity is 1, representing a particle with no convex regions (Fig. 3c).

b) Laboratory procedures

QicPic™ runs under a dry mode (GRADIS) for coarse particles and a wet mode for fine particles. The wet mode (LIXELL) was used. The procedure consists of circulating di-ionised water together with sediment so that the particle shape and size descriptors are captured. At first, the parts were cleaned by circulating de-ionised water. This was followed by adding 0.5g of sediment to a beaker with de-ionized water. A magnetic stirring base was used to keep the sediment suspended. The beaker, pump, and the QicPic™ were connected during the procedure, and the water with suspended sediment was forced to circulate for 5 minutes, after which the measurements were conducted. The computer control panel was set to the required configurations, such as the specific lens for the particle size (which is M4 (2-682µm) in this study), capturing the temporal length of the test (40s in this study), and any repeat tests (3 times in this study).

In order to validate the laboratory measurements, a control experiment was conducted with 100 µm glass beads. This revealed a particle size of 127.59 µm, aspect ratio 0.962, convexity 0.926 and sphericity 0.897. For perfectly spherical beads the particle shape descriptors should have equaled 1. As a limitation of the method, D_{50} represents the median of the particle shape distribution. As such, two different sediment samples with a wider or narrower particle shape distribution may yield the same D_{50}.

c) Seismic interpretation

We used a three-dimensional (3D) pre-stack depth migrated (PSDM) seismic volume covering part of the Nankai Trough accretionary wedge. The studied region of the Nankai Trough is located at a water depth between 1750 m to 3200 m (Fig. 2). The interpreted seismic volume has an inline spacing of 12.5 m, for a crossline spacing of 18.75 m. It was acquired with a 2-source array with four receiver cables spaced 150 m apart. The processing of the seismic volume included pre-stack multiple removal and data conditioning that included amplitude recovery, time-variant filtering, and predictive deconvolution. A 3D pre-stack depth migration followed this latter sequence (Moore et al., 2009). Seismic resolution approaches 6 m at the depth of deposition of MTDs A and B, and based on the dominant wavelength of ~ 24 m observed on synthetic logs (Fig. 2b). Also, for this work, a series of seismic horizons were interpreted below the base of the interpreted MTDs A and B, which were drilled during IODP Expedition 333 (Expedition 333 Scientists, 2011).

4. Results and Discussion

a) Morphometric signature

A detailed analysis of the average value and standard deviation for particle size, aspect ratio, convexity and sphericity were completed for MTDs A, B and the undisturbed slope deposits (Fig. 4). Given very few samples were available for borehole C0018A the analysis is focused on samples MTD B and undisturbed slope. Particle morphology reveals that MTD B and the undisturbed slope have similar particle size characteristics, whereas sediment underlying MTD B has a larger particle size and relatively smaller shape attributes (Fig. 4). At IODP borehole C0021B, MTD B shows a particle size of 15.25 (±2.82) μm, an aspect ratio of 0.708 (±0.009), convexity of 0.869 (±0.013) and a sphericity of 0.870 (±0.014). Undisturbed slope sediment above MTD B shows particle size of 13.95 (±2.50) μm, an aspect ratio of 0.707 (±0.008), a convexity of 0.863 (±0.017), and a sphericity of 0.871 (±0.016).

At IODP borehole C0018A, MTB B presents a particle size of 20.21 (±5.68) μm, an aspect ratio of 0.707 (±0.009), convexity of 0.878 (±0.018), and a sphericity of 0.860 (±0.022). For the overlying (undisturbed) slope deposits, particle size is 17.64 (±3.71) μm, aspect ratio approaches 0.708 (±0.013), convexity is 0.870 (±0.018) and sphericity 0.855 (±0.033). These results suggest an increase in the particle size for MTD B at borehole C0018A, indicating that the longer travel distance may have entrained coarser turbidite material (Unit II) in this same MTD. No perceptive differences in the particle shape attributes between the two IODP boreholes were found in our analyses.

Fig. 5 shows the variation of particle shape with size for MTD B in both IODP boreholes. The shape parameters remain similar with depth, especially for a size range of 20-40μm. It also shows the particles within the same size range (10-20μm) in the two IODP boreholes have similar particle shapes. For comparison, Leighton Buzzard Sand, a sub-rounded quartz sand and frequently tested standard material (e.g. Senetakis et al., 2013) achieves a sphericity in the range 0.881 – 0.894 (for particle sizes 63 – 600 μm) and aspect ratio in the range 0.729 – 0.761 (Saulick et al., 2018). Compared to Leighton Buzzard sand, the sediments in IODP boreholes C0018A and C0021B are more angular (i.e., have a lower sphericity) and more elongated (i.e., have a lower aspect ratio). The mean values of morphological properties are summarized in Table 1.

b) Similarity between the morphometric signatures on slope and landslide sediment

The similarity between the morphometric signatures of the undisturbed sediment and MTD B, for the two IODP Sites analysed, suggests that: (1) sediment was remobilized from previously existing slope deposits, and (2) limited interaction or contact between the particles during the MTD movement despite their estimated travel distance of 5 km (Moore and Sawyer, 2016). This indicates that, in certain fluidized submarine landslides, particle shape is more influenced by the original source area (and nature) of particles than their transport history. Therefore, in the study area, the limited change in particle attributes is assumed to be intrinsically linked to the small particle size of the sediments (< 100 μm). As the link between the particle morphology changes with transport cannot be directly established, an argument is created to explain the limited or lack of particle morphology changes based on the available and related literature.

Particle breakage is more common in larger particles. The smallest documented particle size for breakage is approximately 300 μm (Nakata et al., 2001; Altuhafi & Coop, 2011), a value greater than the average particle size for MTD B (20 μm). Particle breakage has been

associated to particle size, particle shape, mineralogy and high normal stresses. Particle breakage thus increases with particle size, particle angularity and normal stress, and is frequently associated with carbonate or fossiliferous particles. From ring-shear tests in weathered granitic sands (Sassa et al., 1996), breakage has also been observed for particles with a minimum diameter of 1 mm and from normal stress of 300 kPa. In carbonate sand (Zhang et al., 2017), breakage was observed for particles with a minimum diameter of 600μm and from normal stress of 400kPa. Other crushability tests were conducted successfully down to a minimum of 300 μm (Coop et al., 2004).

Smaller particles have greater intrinsic strength. In single particle breakage experiments, Lee (1992) showed smaller particles to sustain higher tensile strengths. Shear tests on sand particle pairs (1.18-3.50 mm) with different mineralogies (Nardelli and Coop, 2017) showed that the coefficients of inter-particle friction are related to the surface roughness of particles and their composition. Particle damage could be observed in the proximity to the contact region between the two particles for those materials characterized by lower hardness, while no visible effects could be identified for harder sands (e.g. quartz sand). These tests are usually performed by applying small confining forces during shearing (1-10 N), which leads to pressures at particle contacts that can be very high (in the order of magnitude of tens to hundreds of MPa). The minor change of the particle characteristics during the transport and deposition processes is supported by the relatively high hardness of volcanic glass and other typical constituents of volcanic ash, from feldspars to mafic minerals all with a Mohs scale hardness of 5 to 6, although this latter classification is only qualitative (e.g. Tabor, 1954).

A fluidization mechanism is proposed to explain the limited particle attributes changes observed in Nankai. In this mechanism, the movement of the low density and saturated marine sediment leads to the development of excess pore water pressure during landslide movement, inhibiting particle-to-particle contact and subsequent particle shape and size changes. This mechanism is supported by a low effective stress (submerged conditions), low compressibility of water, and putatively reflects a relatively high speed of movement (Moore and Sawyer, 2016). This relatively fast movement maintains and enhances pore water pressure. An intense tectonic environment with uplift, local slope tilting, and high sedimentation rates, will also limit the consolidation of the deposits. The calculation of the effective stress σ' below the sea floor in case of fully saturated soil, following the Terzaghi's principle: $\sigma' = \sigma - u$, where σ is the total stress and u is the pore water pressure, also shows that these values are very low (within the order of magnitude of few hundreds of kPa), reflecting the relatively shallow depth of burial of MTDs A and B. This can be also regarded as a possible cause of the very limited changes in particle characteristics with depth.

c) Particle shape and its dependency on the emplacement mechanisms of submarine landslides

The limited dependency of particle shape on size can also be linked to the nature of the particles rather than the transport history. For the transport history, the particle attributes alteration in the natural environment has been mostly explored in the wind erosion, fluvial and beach dynamics literature. Kuenen (1960) found positive relationships between rates of aeolian abrasion and increasing particle size, angularity and surface roughness. However, these dependencies were not found in this study. If any dependency of shape on size can be argued from Fig. 5, then it could be linked to the existence of particles of different nature, from volcanic ash to microfossils, resulting in unique combinations of particle size and shape. From the SEM images in Figs. 6 (a) and (b), which refer to sediments sampled from IODP Site C0021 at the depths of 100-101 m and 134.5-135.5 m below sea floor, it can be observed that the samples show a large presence of microfossils. Moreover, the sediment

microstructure can be classified as dispersed turbostratic (Fig. 6b), with a close-packed structure, very little interdomain microvoids and cavities and a random overall arrangement, following the sediment structure classification proposed by Sides and Barden (1971). This favours the latter explanation and stresses the dependency of particle properties on 'inherited' properties of the landslides' source areas, rather than their run-out distances and emplacement process. Hence, submarine landslides in Nankai reflect local sources of sediment and marked remobilization of older slope strata. Conversely, less mature, angular sediment should correlate with more dynamic landslide movements, and less mature (i.e. coarser) source material.

5. Conclusions

The morphometric analysis of sediment particles from a mass-transport deposit from the Nankai Trough (Japan) provides an insight into the mobility mechanisms of submarine landslides. Measurements of particle sphericity, convexity and aspect ratio in 200 samples revealed limited differences in the particle attributes between two boreholes and the overlying sediments. It is hypothesized that the finer nature of the sediments, their low density and saturated condition constrains particle-to-particle interaction and subsequent particle attribute changes during mass transport. The low values of effective stress calculated below the sea floor despite the very large depth of the samples (2.7-3km) supports our findings of very limited variation in the particle characteristics along the depth of the boreholes. As for a possible relationship between particle shape and size, the coexistence of microfossils and volcanic ash may have resulted in a unique combination of particle size and shape.

Acknowledgements

This research used samples and data provided by the Integrated Ocean Drilling Program (IODP). Experimental tests were partially supported by the Research Grants Council of Hong Kong; grant T22-603/15-N. Thank you to Dr Yunesh Saulick for support with the QicPic.

References

Alves, T. M., Strasser, M. and Moore, G. (2014). Erosional features as indicators of thrust fault activity (Nankai Trough, Japan). Marine Geology 356, pp. 5-18.

Altuhafi, F. N. and Coop, M. R. (2011). Changes to particle characteristics associated with the compression of sands, Geotechnique, vol. 61(6), pp. 459–471.

Bo, M. W., Arulrajah, A., Sukmak, P. and Horpibulsuk, S. (2015). Mineralogy and geotechnical properties of Singapore marine clay at Changi. Soils and Foundations, vol. 55(3), pp. 600-613.

Blaker, O., Carroll, R., L'Heureux, J. S. and Klug, M. (2016). Characterisation of Halden silt. Proceedings of the 5th International Conference on Geotechnical and Geophysical Site Characterisation. Vol. 2, pp. 975-980. Sydney, Australia.

Bullard, J.E., McTainsh, G.H. and Pudmenzky C. (2004). Aeolian abrasion and modes of fine particle production from natural red dune sands: an experimental study. Sedimentology 51 (5), 1103-1125.

Coop, M. R., Sorensen, K., Freitas, T. B. and Georgoutsos, G. (2004). Particle breakage during shearing of a carbonate sand. Geotechnique, vol. 54(3), pp. 157–163.

Expedition 333 Scientists (2011). Expedition 333 Scientists NanTroSEIZE Stage 2: subduction inputs 2 and heat flow, IODP Preliminary Reports 333, 10.2204/iodp.pr.333.2011

Expedition 338 Scientists (2013). NanTroSEIZE plate boundary deep riser 2, IODP

Preliminary Reports 338, 10.2204/iodp.pr.338.2013

Gulick, S.P.S., et al. (2010). Rapid forearc basin uplift and megasplay fault development from 3D seismic images of Nankai Margin off Kii Peninsula, Japan. Earth and Planetary Science Letters, 300(1-2), 55-62.Kimura, G., Moore, G.F.; Strasser, M.; Screaton, E.; Curewitz, D.; Streiff, C. and Tobin, H. (2011). Spatial and temporal evolution of the megasplay fault in the Nankai Trough: Geochemistry, Geophysics, Geosystems, vol. 12, Q0A008, 18 p.

Kuenen P.H. (1960). Experimental abrasion 4: eolian action. Journal of Geology, Vol. 68, 427-449.

Lee D.M. (1992). The angles of friction of granular fills. The University of Cambridge, PhD dissertation.

Moore, G.F., Park, J.-O., Bangs, N.L., Gulick, S.P., Tobin, H.J., Nakamura, Y., Sato, S., Tsuji, T., Yoro, T., Tanaka, H., Uraki, S., Kido, Y., Sanada, Y., Kuramoto, S., and Taira, A.. (2009). Structural and seismic stratigraphic framework of the NanTroSEIZE State 1 transect, NanTroSEIZE Stage 1: Investigations of Seismogenesis, Nankai Trough, Japan: Proceedings Integrated Ocean Drilling Program 314/315/316.

Moore, Z.T. and Sawyer, D.E. (2014). Data report: particle size analysis of Nankai Trough sediments, IODP Expedition 338 Site C0021, Proc. IODP, Volume 338.

Moore, Z.T. and Sawyer, D.E. (2016). Assessing post-failure mobility of submarine landslides from seismic geomorphology and physical properties of mas-transport deposits: An example from seaward of the Kumano Basin, Nankai trough, offshore Japan. Marine Geology vol. 374, pp. 73–84

Nakata, Hyodo M., Hyde, A.F.L., Kato, Y. and Murata, H. (2001). Microscopic particle crushing of sand subjected to high pressure one-dimensional compression. Soils & Foundations, vol. 41(1), pp. 69-82.

Nardelli, V. and Coop, M.R. (2017). The experimental contact behaviour of natural sands: normal and tangential loading. Submitted to Geotechnique.

Ohtsubo, M., Egashira, K., Koumoto, T. and Bergado, D. T. (2000). Mineralogy and chemistry, and their correlation with the geotechnical index properties of Bangkok clay: comparison with Ariake clay. Soils and Foundations, vol. 40(1), pp. 11-21.

Saulick, Y., Lourenco, S.D.N., Baudet, B.A., Woche, S. and Bachmann, J. (2018). Physical-properties controlling water repellency in synthesised granular solids, European Journal of Soil Science 10.1111/ejss.12555

Sassa, K.; Fukuoka, H.; Scarascia-Mugnozza, G. and Evans, S. (1996). Earthquake-induced –landslides: distribution, motion and mechanisms. Soils & Foundations, Special Issue for the Great Hanshin Earthquake Disaster, pp 53−64.

Senetakis, K.; Coop, M.R. and Todisco. M.C. (2013). The inter-particle coefficient of friction at the contacts of Leighton Buzzard sand quartz minerals. Soils and Foundations 53, No. 5, 746-755.

Sides, G. and Barden, L. (1971). The microstructure of dispersed and flocculated samples of kaolinite, illite and montmorillonite. Canadian Geotechnical Journal, 8, 391-399.

Skempton, A. W. (1985) Residual strength of clays in landslides, folded strata and laboratory. Geotechnique, vol. 35(1), pp 3-18.

Strasser, M.; Moore, G.F; Kimura, G., Kopf, A.J.; Underwood, M.B., Guo, J. and Screaton, E.J. (2011). Slumping and mas-transport deposition in the Nankai fore arc: evidence from IODP drilling and 3-D reflection seismic data. Geochem. Geophys. Geosyst. 12 (5), Q0AD13.

Strasser, M., et al. (2009). Origin and evolution of a splay fault in the Nankai accretionary wedge. Nature Geoscience 2, 648-652.

Tabor, D. (1954). Mohs's Hardness Scale - A Physical Interpretation. Proc. Phys. Soc. B 67 249

Wadell, H. (1933). Sphericity and roundness of rock particles. Journal of Geology, 41, 310-330.

Wafid, A.M., Sassa, K., Fukuoka, H. and Wang G.H. (2004). Evolution of Shear-Zone Structure in Undrained Ring-Shear Tests, Landslides, vol. 1(2), 101–112.

Wiemer, G. and Kopf, A. (2017), On the role of volcanic ash deposits as preferential submarine slope failure planes. Landslides, vol. 14(1), 223–232.

Wiemer, G.; Moernaut, J.; Stark, N; Kempf, P.; De Batist, M.; Pino, M.; Urrutia, R.; Ladron de Guevara, B.; Strasser, M. and Kopf, A. (2015). The role of sediment composition and behavior under dynamic loading conditions on slope failure initiation: a study of a subaqueous landslide in earthquake-prone South-Central Chile. Int J Earth Sci (Geol Rundsch), Vol 104(5), pp. 1439-1457.

Zhang, X; Baudet, B.A.; Hu, W. and Xu, Q. (2017). Characterisation of the ultimate particle size distribution of uniformand gap-graded soils. Soils and Foundations, vol 57, pp 603-618.

Tables and Figures

Table 1 Summary of mean values for the particle morphological properties

Morphological properties	Sediment				
	MTDB		Undisturbed deposits		Leighton Buzzard Sand (for reference)
	C0021B	C0018A	C0021B	C0018A	
Mean particle size (μm)	15.25	20.21	13.95	17.64	63-600
Mean aspect ratio	0.708	0.707	0.707	0.708	0.729-0.761
Mean convexity	0.869	0.878	0.863	0.87	-
Mean sphericity	0.87	0.86	0.871	0.855	0.881-0.894

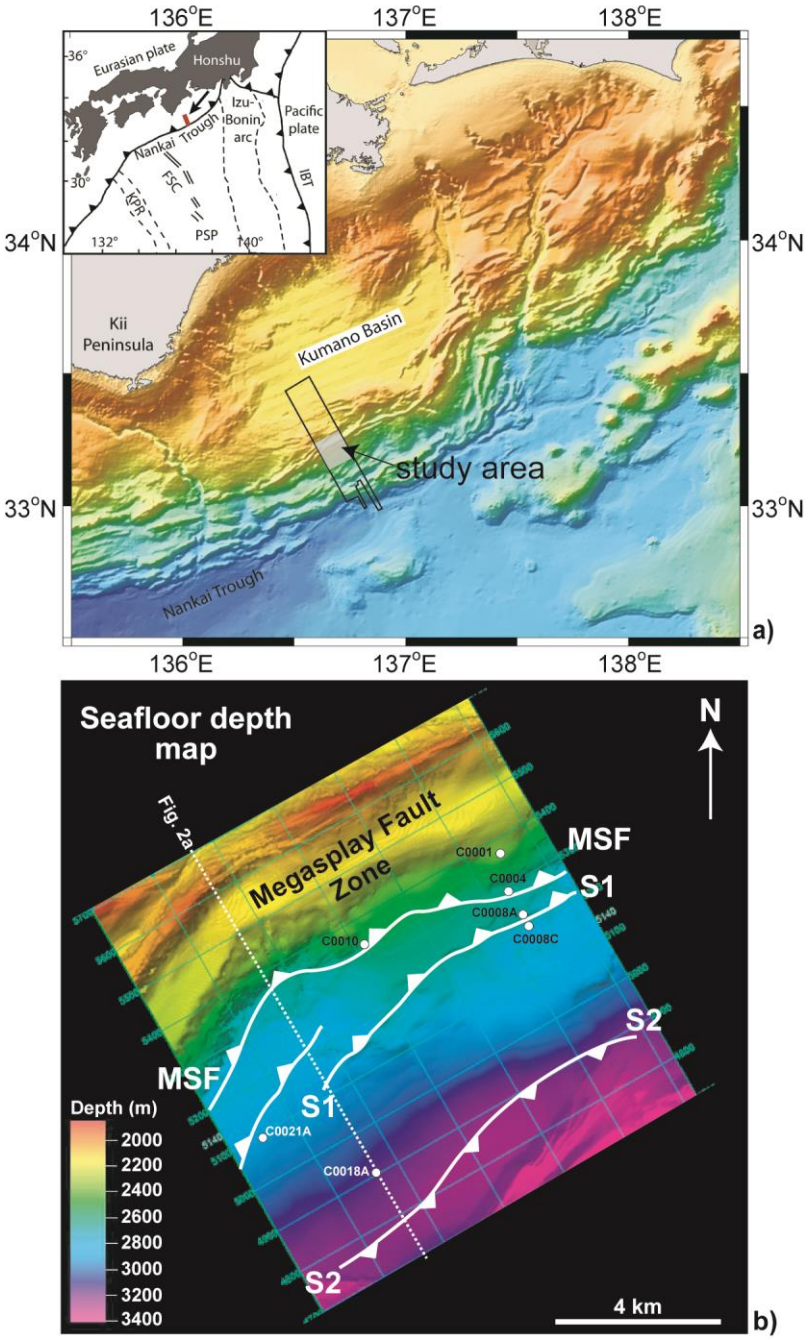

Figure 1 – (a) Location of the study area and Kumano Transect across the Nankai Trough accretionary wedge. Arrow in inset indicates the position of the interpreted 3D seismic volume in SE Japan. (b) Seafloor map showing the location of main structural features, IODP sites, boreholes and interpreted seismic volume. MSF - Megasplay Fault. S1 and S2 refer to the main thrust faults shown in Fig. 2a (modified from Alves et al., 2014).

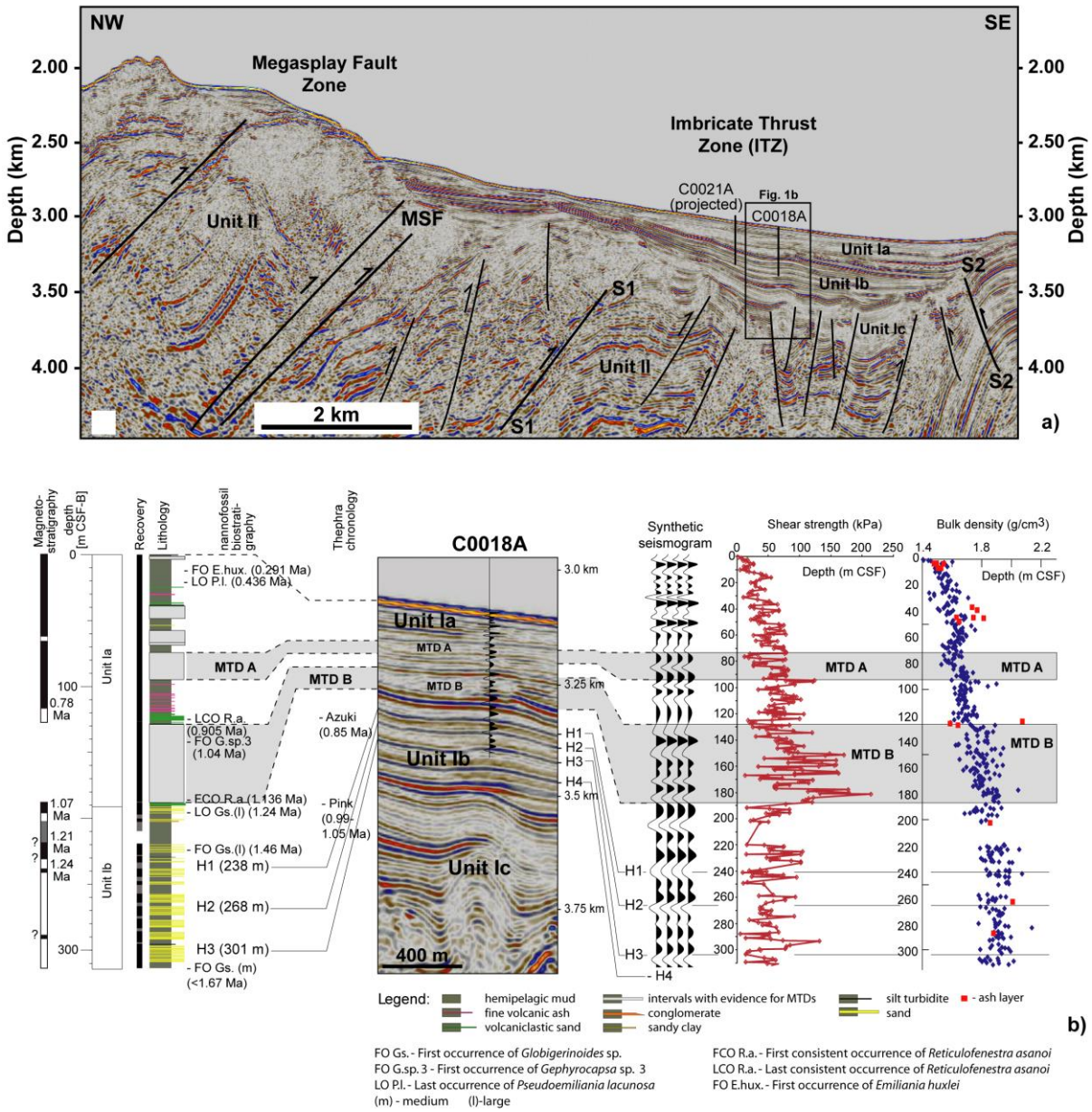

Fig. 2: (a) Depth-migrated seismic profile (inline 2315) crossing the Nankai continental slope. The Fig. highlights the location of structural zones and thrust faults S1 and S2 (Moore et al., 2009; Alves et al., 2014). The relative location of IODP boreholes C0018A and C0021A (the same location as borehole C0021B) are shown in the Fig. (b) Sedimentary log of IODP boreholes C0018A tying MTDs A and B with synthetic seismic, shear strength and bulk density data.

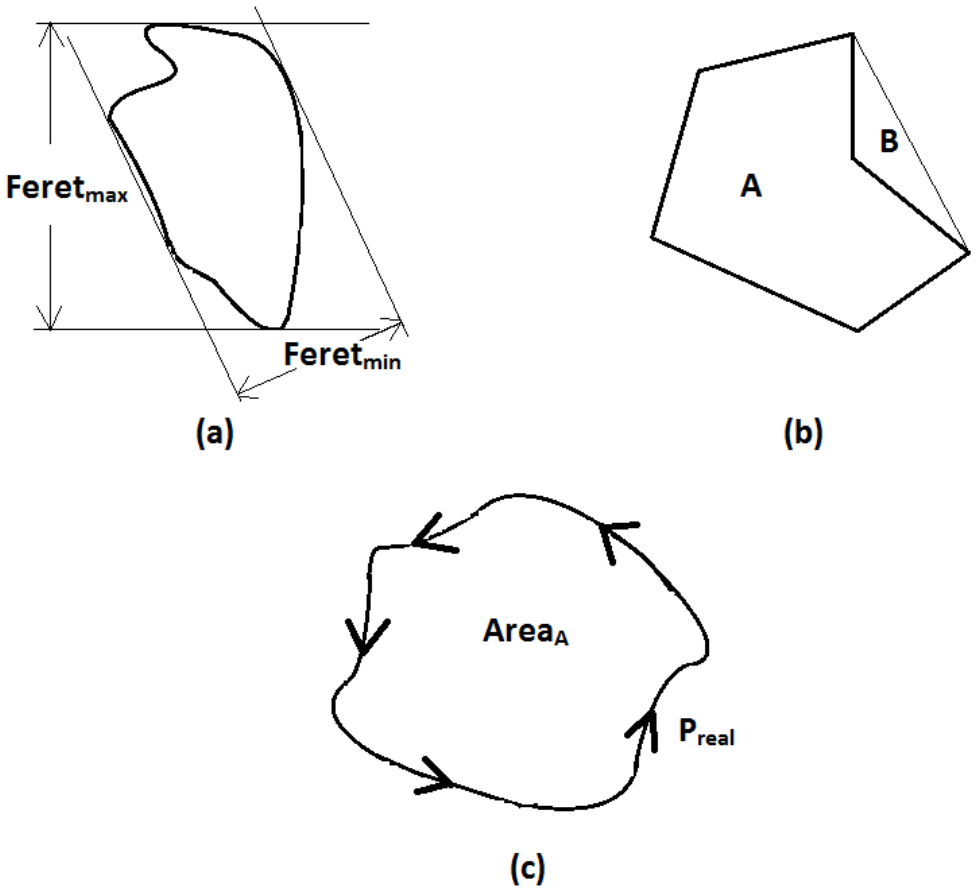

Fig. 3: Schematic particle shape descriptors, a) aspect ratio (ratio of minimum to maximum Feret diameters), b) convexity (ratio between the projected area of a particle A and the area of a convex shape - B), c) sphericity (ratio of the perimeter of the equivalent circle by the actual perimeter - P_{real})

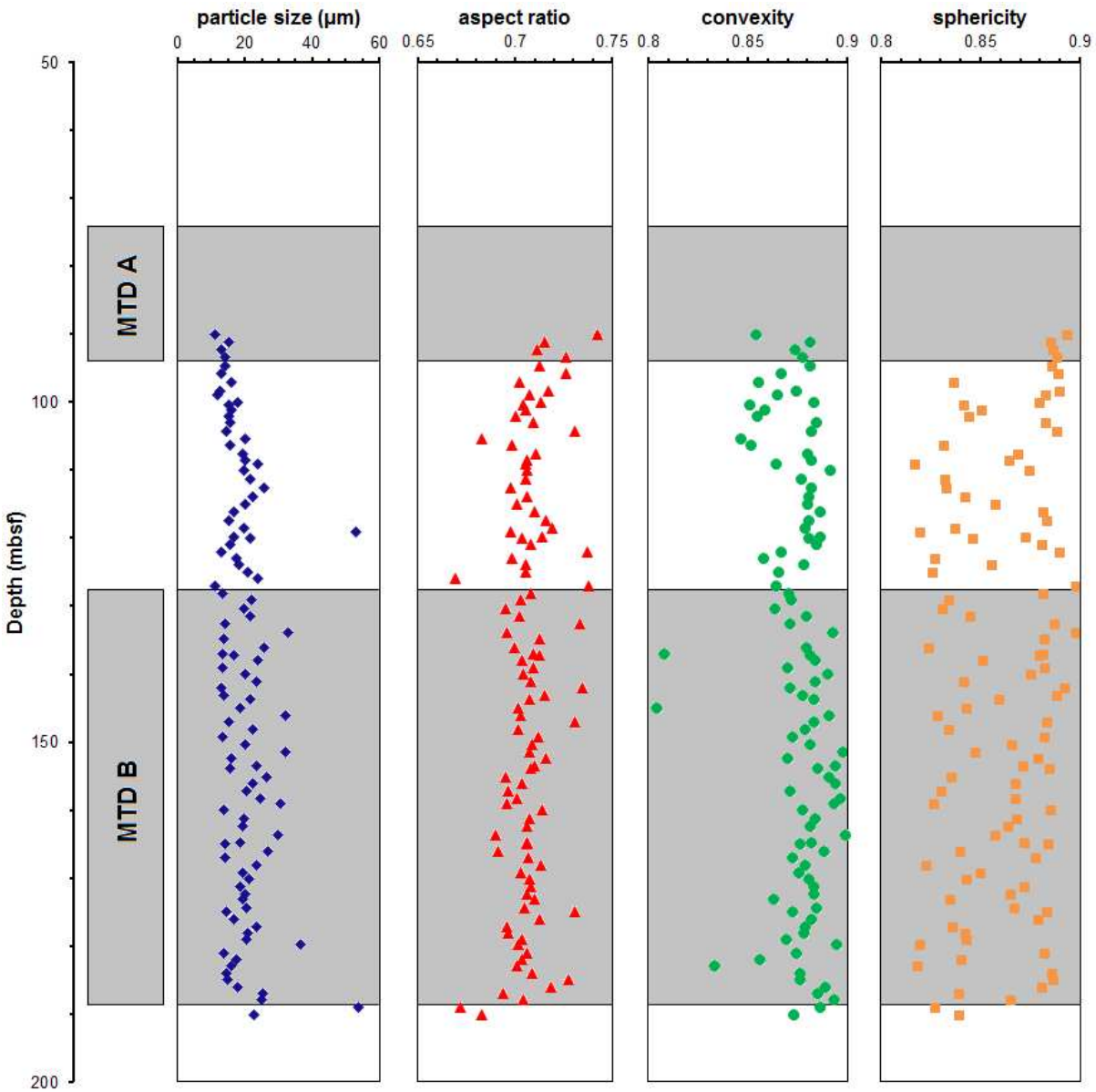
particle size (µm)
0
20
40
60
aspect ratio
0.65
0.7
0.75
convexity
0.8
0.85
0.9
sphericity
0.8
0.85
0.9
50
100
150
200
Depth (mbsf)
MTD A
MTD B

(a)

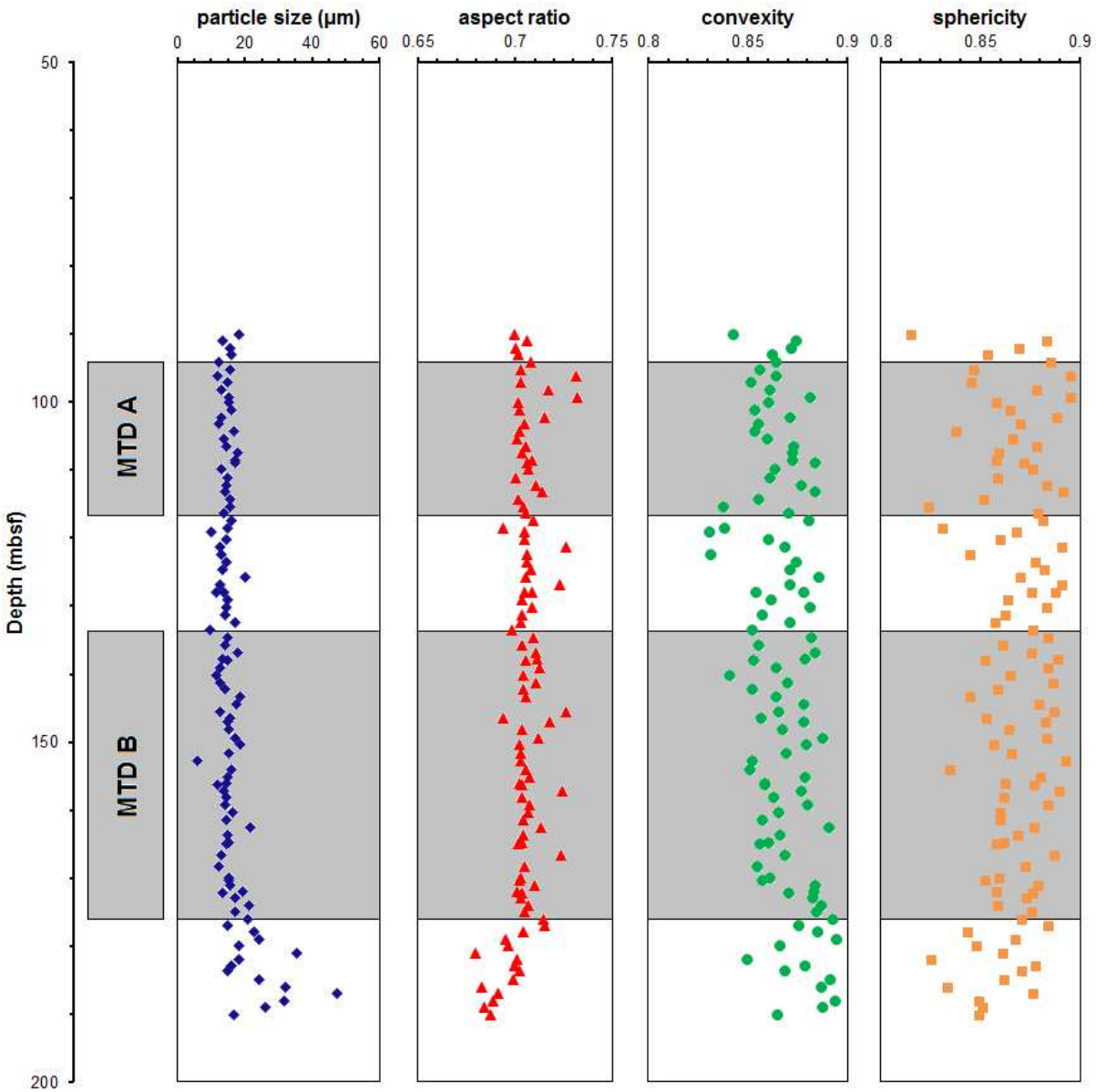

(b)

Fig. 4: Particle size and shape descriptors with depth, a) Borehole C0018A, b) Borehole C0021B

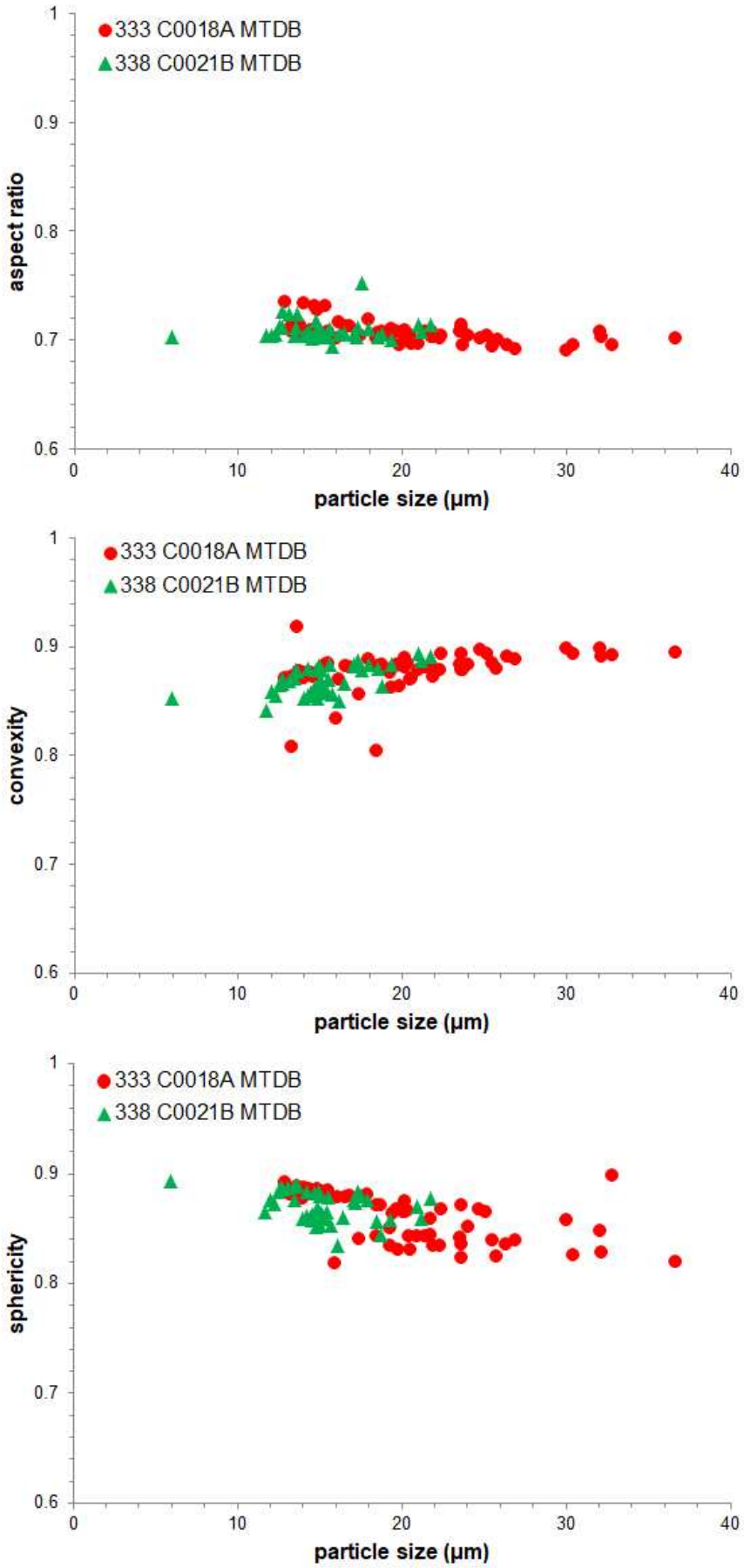

Fig. 5: Correlation between the particle size and shape descriptors for MTDB

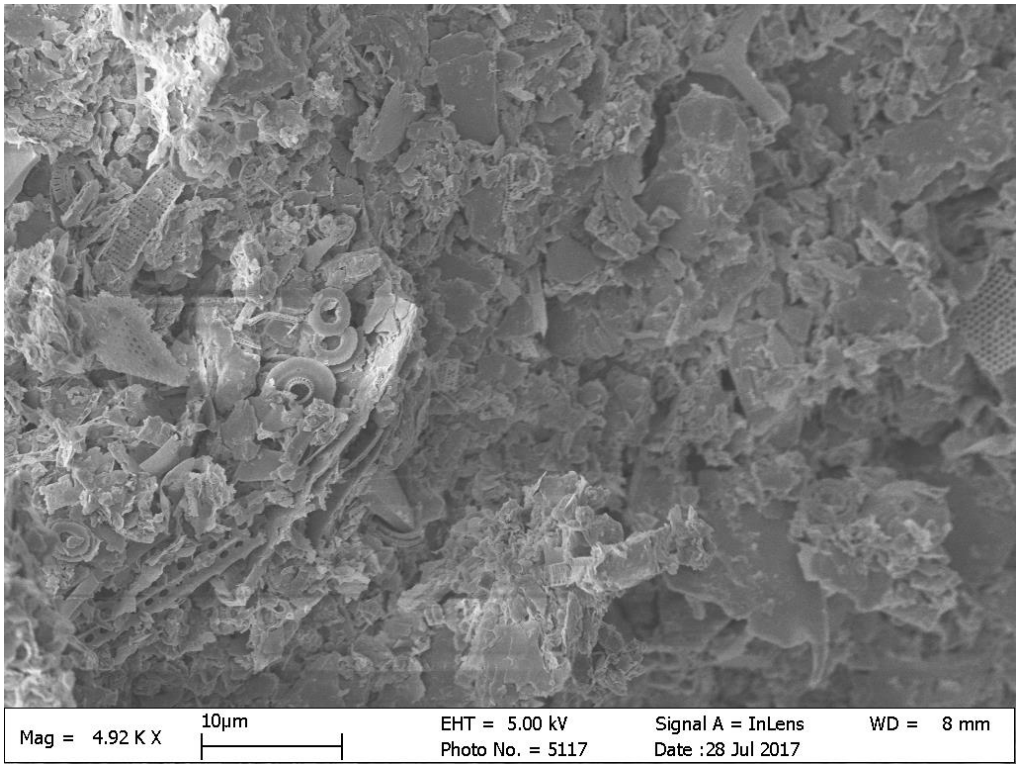

(a)

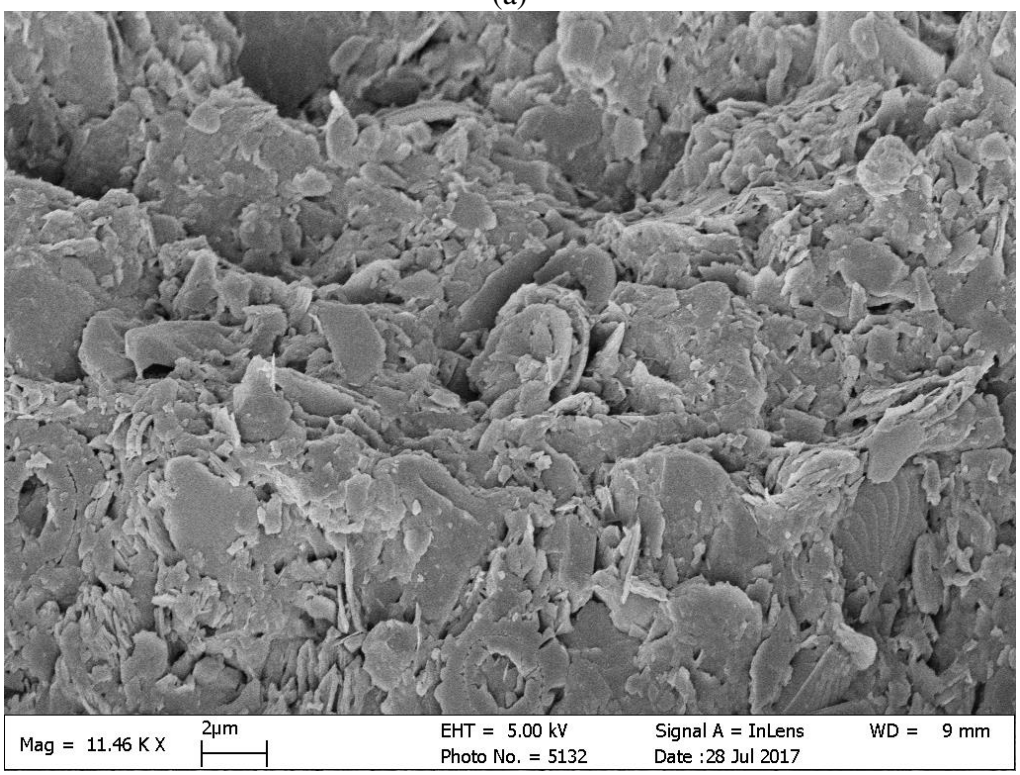

(b)

Fig. 6: SEM images of the soil microstructure of two undisturbed samples taken from Site C0021 at the depth 100-101m below seafloor (a) and 134.5-135.5m (b)